analytical chemistry

ARTICLE

pubs.acs.org/ac

Temperature Modulation and Quadrature Detection for Selective Titration of Two-State Exchanging Reactants

K. Zrelli,[†] T. Barilero,[†] E. Cavatore,[‡] H. Berthoumieux,[†] T. Le Saux,[*,†] V. Croquette,[‡] A. Lemarchand,[*,§] C. Gosse,[*,∥] and L. Jullien[*,†]

[†]Département de Chimie, Ecole Normale Supérieure, UMR CNRS-ENS-UPMC Paris 06 8640 Pasteur, 24 rue Lhomond, 75231 Paris Cedex 05, France

[‡]Laboratoire de Physique Statistique, Département de Physique, Ecole Normale Supérieure, UMR CNRS 8550, 24 rue Lhomond, 75231 Paris Cedex 05, France

[§]Laboratoire de Physique Théorique de la Matière Condensée, Université Pierre et Marie Curie Paris06, UMR CNRS-UPMC 7600, 4 place Jussieu, 75252 Paris Cedex 05, France

[∥]Laboratoire de Photonique et de Nanostructures, LPN-CNRS, route de Nozay, 91460 Marcoussis, France

Supporting Information

ABSTRACT: Biological samples exhibit huge molecular diversity over large concentration ranges. Titrating a given compound in such mixtures is often difficult, and innovative strategies emphasizing selectivity are thus demanded. To overcome limitations inherent to thermodynamics, we here present a generic technique where discrimination relies on the dynamics of interaction between the target of interest and a probe introduced in excess. Considering an ensemble of two-state exchanging reactants submitted to temperature modulation, we first demonstrate that the amplitude of the out-of-phase concentration oscillations is maximum for every compound involved in a reaction whose equilibrium constant is equal to unity and whose relaxation time is equal to the inverse of the excitation angular frequency. Taking advantage of this feature, we next devise a highly specific detection protocol and validate it using a microfabricated resistive heater and an epifluorescence microscope, as well as labeled oligonucleotides to model species displaying various dynamic properties. As expected, quantification of a sought for strand is obtained even if interfering reagents are present in similar amounts. Moreover, our approach does not require any separation and is compatible with imaging. It could then benefit some of the numerous binding assays performed every day in life sciences.

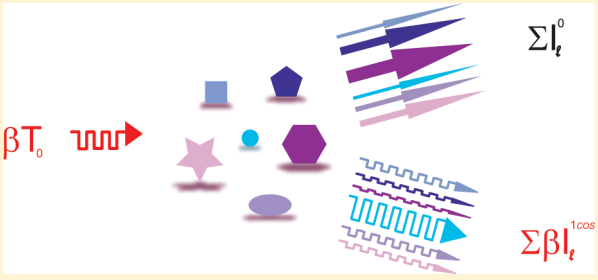

INTRODUCTION

Quantifying a given species in a complex medium of living origin is currently encountered in many medical and pharmaceutical activities such as molecular diagnosis[1,2] and drug screening.[3] Moreover, extensive characterization of the cellular content is the workhorse of scientific fields such as genomics, proteomics, and metabolomics. Yet these analytical tasks represent a tremendous challenge, as crude biological samples typically contain 10^4-10^6 components of the same kind (e.g., RNAs, proteins) at concentrations covering up to 10 orders of magnitude.[1,4,5] Improvement in assay selectivity is therefore required to avoid as much as possible the cumbersome pretreatments today necessary prior to any specific detection.

Directly "counting" intrinsic labels such as functional groups is not appropriate to investigate the considered mixtures because they are mostly made of biopolymers that share the same building blocks in the same proportions. In fact, this type of approach results in spectral crowding, and unambiguous species identification can be achieved only through coupling with methods emphasizing physicochemical criteria (e.g., separation for mass spectrometry[6] or correlation analysis for IR absorption[7,8]). Besides such complicated multidimensional analyses, titration is then a valuable strategy because one just has to observe a single reagent selectively probing the compound of interest. Furthermore, in the present context there it benefits from the high specificity that characterizes molecular recognition in biology.[9]

Binding assays, which rely on thermodynamics for discrimination, are actually widespread. Whereas "mix-and-read" tests are homogeneous and consequently convenient, the advent of microarrays has yielded unprecedented multiplexing capabilities, with thousands of titrations being performed in parallel.[10−14] However, species concentrations are often overestimated because labeling reagents are insufficiently rinsed away or because nonspecific adsorption onto solid supports is poorly controlled.[9,12,14,15] Additionally, in a mixture of similar components, a single probe is anticipated to display close affinities for several targets.[11] Thus,

Received: October 2, 2010
Accepted: January 16, 2011
Published: February 28, 2011

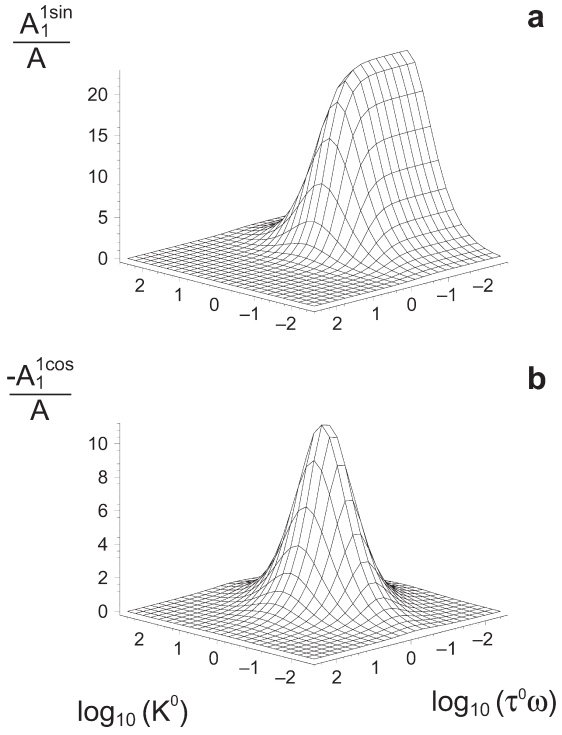

Figure 1. Theoretical computation of the response of a two-state exchanging reactant $A_1 \rightleftharpoons A_2$ submitted to thermal harmonic forcing. The normalized amplitudes of the in-phase and out-of-phase oscillations in A_1 concentration, A_1^{1sin}/A and $-A_1^{1cos}/A$, respectively, are plotted versus the equilibrium constant K^0 and the adimensional relaxation time $\tau^0\omega$ for $\Delta H/RT_0 = -90$. See eqs 5 and 6.

to overcome such limitations, detection selectivity has to be improved. We here propose to increase the number of discriminating parameters by relying on kinetics:[16] for instance, at least two independent rate constants, instead of the sole thermodynamic one, are associated with every titration reaction. We have already implemented such an approach to devise highly efficient separative protocols[17−21] and we shall now demonstrate its relevance for quantitative analysis.

To reveal chemical dynamics, we have retained the principle of a perturbation that periodically forces the system out of equilibrium. This strategy provides rate constants and mechanisms in relaxation methods,[22,23] whereas it is used to resolve overlapping bands in spectroscopy[23−25] and to enhance the signal-to-noise ratio in biodetection.[26,27] More practically, we have chosen temperature as the most versatile parameter for periodic excitation.[28−30] As a matter of fact, thermodynamic and kinetic constants of biologically relevant processes significantly depend on it—namely, the values of the reaction enthalpies typically lie in the 20−200 kJ·mol^{-1} range.[31−33] In addition, temperature modulations of weak amplitude are noninvasive, compatible with in vivo imaging,[34] and easy to implement, either globally (at the scale of a microsystem)[26,34−37] or locally (in the close surroundings of a nanoparticle).[38−40]

THEORY

We consider a titration in which an analyte A_1 reacts with a probe P to form a product A_2, the forward and backward rate constants being respectively denoted k_+^P and k_-. If the concentration P is such that P is in great excess, we can model the reaction as a two-state exchange:

$$A_1 \underset{k_-}{\overset{k_+}{\rightleftharpoons}} A_2 \qquad (1)$$

with $k_+ = k_+^P P$. A sinusoidal modulation of the temperature T is then applied around T_0, at angular frequency ω and with a small amplitude βT_0:

$$T = T_0[1 + \beta \sin(\omega t)] \qquad (\beta \ll 1) \qquad (2)$$

Following Arrhenius, we have $k_\pm(T) = r_\pm \exp(-E_\pm/RT)$, where R is the ideal gas constant. As both the pre-exponential factors $r_\pm$ and the activation energies $E_\pm$ are here assumed to not vary with T, a first-order expansion in the perturbation yields $k_\pm(t) = k^0_\pm [1 + \beta\varepsilon^0_\pm \sin(\omega t)]$ with $k^0_\pm = r_\pm \exp(-\varepsilon^0_\pm)$ and $\varepsilon^0_\pm = E_\pm/RT_0$.[23,29] Beyond the relaxation time $\tau^0 = 1/(k^0_+ + k^0_-)$, one enters into the forced and permanent regime where the concentration $A_i(t)$ in each species A_i obeys[28]

$$A_i(t) = A_i^0 + \beta[A_i^{1sin} \sin(\omega t) + A_i^{1cos} \cos(\omega t)] \qquad (3)$$

In the latter equation, A_i^0 is the A_i concentration at chemical equilibrium at T_0:

$$A_1^0 = A - A_2^0 = \frac{A}{1 + K^0} \qquad (4)$$

where A is the total concentration in the $\{A_1, A_2\}$ couple and $K^0 = k^0_+/k^0_-$ is the reaction 1 equilibrium constant at T_0. Moreover, the amplitudes of the oscillating terms at angular frequency ω, in phase and out of phase with the temperature, are respectively given by eqs 5 and 6:

$$A_1^{1sin} = -A_2^{1sin} = -\frac{\Delta H}{RT_0}\frac{K^0}{(1+K^0)^2}\frac{1}{1+(\tau^0\omega)^2}A \qquad (5)$$

$$A_1^{1cos} = -A_2^{1cos} = \frac{\Delta H}{RT_0}\frac{K^0}{(1+K^0)^2}\frac{\tau^0\omega}{1+(\tau^0\omega)^2}A \qquad (6)$$

where $\Delta H = E_+ - E_-$ is the standard enthalpy of the exchange reaction.

Figure 1 displays, for a fixed value of ΔH, the dependence on K^0 and $\tau^0\omega$ of A_1^{1sin}/A and $-A_1^{1cos}/A$. Interestingly, the amplitude in quadrature exhibits a single maximum centered on

$$K^0 = 1 \quad \text{and} \quad \tau^0\omega = 1 \qquad (7)$$

with full widths at half-maximum $4\sqrt{2}$ along K^0 and $2\sqrt{3}$ along $\tau^0\omega$. Due to the symmetry of the sinusoidal forcing, a first condition for this "resonance" to occur is that A_1 and A_2 are in equal proportions. Indeed, the temperature modulation then causes the largest relative variations of their concentrations. Second, the reaction relaxation time has to match the oscillation period. In fact, in the $1/\tau^0 \ll \omega$ regime, the exchange is slow compared to the temperature variations, the $\{A_1, A_2\}$ couple has not enough time to respond: both A_1^{1sin} and A_1^{1cos} vanish. Conversely, in the $1/\tau^0 \gg \omega$ regime, the A_1 concentration keeps pace with the thermal excitation: A_1^{1sin} plateaus at its highest values, whereas A_1^{1cos} cancels.

The existence of a peaked response for A_1^{1cos} is significant to quantify a given targeted couple $\{A_{t1}, A_{t2}\}$ in an unknown mixture of reactive compounds $\{A_{l1}, A_{l2}\}$ associated with different values of equilibrium constants K_l^0, relaxation times τ_l^0, and total concentrations A_l.[41] As an illustration, we shall provide some calculations for titrations performed in a simplified case

dx.doi.org/10.1021/ac1026034 |Anal. Chem. 2011, 83, 2476–2484

where we assume that (i) only the A_{l1} species participate in the overall signal, for instance, because fluorescence emission is quenched in A_{l2}; (ii) the output contribution of each compound linearly depends on its concentration A_{l1} with a proportionality factor unique to all the A_{l1}; and (iii) all exchanges have a similar $\Delta_l H$ value: the latter parameter is indeed expected to vary just over 1−2 orders of magnitude, whereas K_l^0 and τ_l^0 can typically span 10 orders of magnitude because of their exponential dependence on the reaction enthalpy. In the absence of any information about composition, the target concentration has to be evaluated by presuming that the signal from the whole sample is solely due to the sought for reactant. Therefore, the titration result A_t^{tit} is always an overestimate of A_t. For example, a protocol relying on equilibrium at constant temperature T_0 leads to

$$A_t^{\text{tit-0}} = A_t + \sum_{l\neq t} \frac{(A_{l1}^0/A_l)}{(A_{t1}^0/A_t)} A_l = A_t + \sum_{l\neq t} \frac{(1+K_t^0)}{(1+K_l^0)} A_l \quad (8)$$

Noteworthily, the second component of the right term can hardly be made negligible, which means that the contribution of the species of interest cannot be maximized among those of the interfering compounds. In contrast, looking at the out-of-phase response to a thermal excitation yields

$$A_t^{\text{tit-1cos}} = A_t + \sum_{l\neq t} \frac{(A_{l1}^{1\text{cos}}/A_l)}{(A_{t1}^{1\text{cos}}/A_t)} A_l \quad (9)$$

Provided the eq 7 resonant conditions are satisfied for $\{A_{t1}, A_{t2}\}$, we have $(A_{t1}^{1\text{cos}}/A_t) \gg (A_{l1}^{1\text{cos}}/A_l)$ whenever $l \neq t$ (Figure 1b and Table 1S in the Supporting Information). Thus, the signal issued from the targeted couple can now dominate the one from the other couples. Figure 2 illustrates for various equimolar mixtures the superiority of this second strategy over equilibrium measurements: whereas all the $A_t^{\text{tit-0}}$ values are several times larger than the actual A_t concentration, the discrepancy between $A_t^{\text{tit-1cos}}$ and A_t becomes vanishingly small as soon as the $\{A_{l1}, A_{l2}\}$ depart from $\{A_{t1}, A_{t2}\}$ in the $(K^0, \tau^0\omega)$ plane.

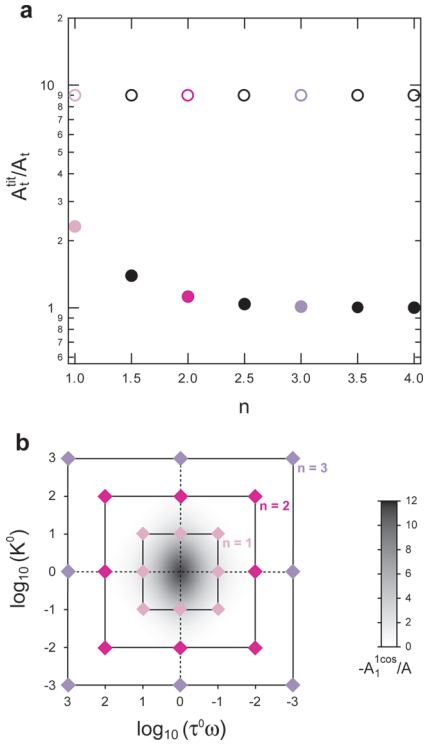

Figure 2. Theoretical computation of the ratio between the titration outcome A_t^{titr} (which assumes that only the sought for reactant is present) and the effective target concentration A_t. (a) Results for both (○) "equilibrium" and (●) "temperature modulation and quadrature detection" methods are compared for seven different equimolar mixtures, which include the targeted two-state exchanging reactant plus eight other interfering couples. In each sample labeled n, the latter species correspond to the eight $(K_l^0, \tau_l^0\omega)$ sets placed on the outer nodes of a 3 × 3 grid centered on $(K_t^0, \tau_t^0\omega) = (1, 1)$ and whose mesh size is n in decimal logarithmic units. (b) Graphical representation in the $(K^0, \tau^0\omega)$ plane of some of the preceding mixtures. Each set of colored diamonds corresponds to a sample with a given n value. Gray levels figure the peak associated with the out-of-phase resonance.

EXPERIMENTAL SECTION

Reagents and Solutions. Solutions were prepared using water purified through a direct-Q5 system(Millipore, Billerica, MA). 4-(2-Hydroxyethyl)-1-piperazineethanesulfonic acid (Hepes), $Mg(OH)_2$, and NaOH were purchased from Sigma−Aldrich (St. Louis, MO).

Poly(dimethylacrylamide) (PDMA) of average molecular mass ~3 MDa, was given by J. Weber (Institut Curie, Paris, France). This polymer was introduced in all solutions to prevent, thanks to dynamic coating, biomolecules adsorption onto the microdevice walls.

The oligonucleotides were synthesized on the 1 μmol scale, conjugated, and double-HPLC-purified by IBA (Göttingen, Germany). With a 5′−3′ orientation, boldface capitals to designate the bases involved in hybridization, and bhq, fam, rhg, and tex to respectively designate the black hole quencher 2, fluorescein, rhodamine green, and Texas red labels, the single-stranded sequences read A_{t1} = rhg-**CTTTGTTTG**; P = AGAGGCCA-T**AAACAAAG**GA; A_{NR} = rhg-T_{11}; A_{MB} = fam-T_7**GATAG**T_{16}**C-TATC**-tex; and M = tex-T_7**GATAG**T_{16}**CTATC**-bhq. The concentration of the stock solutions was estimated by measuring their absorption at 260 nm on a Uvikon-940 spectrophotometer (Kontron, Zürich, Switzerland). This determination was performed at 20 °C and we relied on the molar absorption coefficients provided by the manufacturer.

Thermal Control. To generate temperature oscillations in the solution to be analyzed, we made use of a previously described resistor.[35] This heater, 340 μm × 340 μm large, was micromachined in a 400 nm indium tin oxide (ITO) film of resistivity 10 Ω/□ that had been deposited on a 550 μm thick glass wafer (Figure 3). More precisely, the fabrication was a three-step process: (i) the hot plate feature was defined by optical lithography and transferred into the thin film semiconductor by ion beam etching; (ii) a second photolithography followed by a standard lift-off procedure yielded gold leads that enabled to contact the active zone with the macro-world; (iii) the whole heater was encapsulated in a 800 nm thin layer of silica to prevent any electrochemical degradation of the sample. Once electrical connectors had been welded, the device was completed by assembling the fluidic system: a PDMS stamp including 35 μm large and 10 μm high channels, separated by 20 μm walls.

In operation, the bottom glass surface of the microchip was placed on a 0.4 mm thick copper disk in which a 3 mm large slit had been opened for observation with the objective. This metal holder was itself mounted on an aluminum block thermostated at ±0.2 K with thermoelectric Peltier devices (CP 1.0-63-05

dx.doi.org/10.1021/ac1026034 |Anal. Chem. 2011, 83, 2476–2484

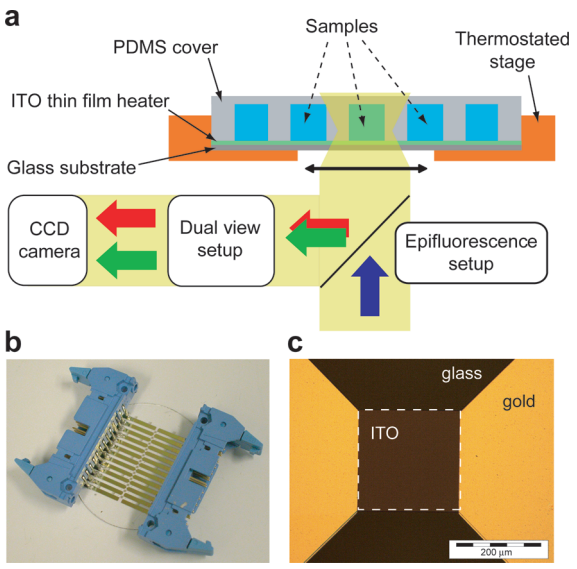

Figure 3. Experimental setup and microsystem used to impose on the sample a temperature modulation of controlled frequency, amplitude, and average value, as well as to observe both the green-emitting analytes and the red-emitting molecular thermometer. (a) General layout. (b) Large-scale view of a 50 mm diameter glass wafer on which 13 ITO resistors of different sizes have been fabricated. (c) Detailed view of a square microheater.

L-RTV; Melcor, Trenton, NJ). The stage temperature was monitored with a TCS610 thermistor (Wavelength Electronics, Bozeman, MT) and the feedback loop was driven by a MPT1000 temperature controller (Wavelength Electronics), which received instructions from the computer through a usb-1208 fs I/O board (Measurement Computing, Norton, MA).

For experiments where thermal excitation was required, we injected a sinusoidal current of peak amplitude 18 mA in the ITO resistor using a function generator, either a DS360 (Standford Research Systems, Sunnyvale, CA) or a 33220A−20 MHz (Agilent, Santa Clara, CA). It resulted in a 0.6−2.4 K modulation in the microfluidic chamber, at a frequency twice the applied electrical one. Actually, a precise calibration of β has been performed for each pulsation ω between 0.54 and 59 rad·s^{-1}: on one hand the current was monitored by measuring with a 54600B−100 MHz oscilloscope (Hewlett-Packard, Santa Clara, CA) the voltage drop across a 47 Ω power resistance (RLP 1%, Vishay-Serfnice, Selb, Germany) connected in series with the device; on the other hand, the amplitude of the temperature oscillations was determined thanks to the ratiometric molecular thermometer MB and to the dual-view epifluorescence setup, as described in Barilero et al.[42]

Furthermore, to control the homogeneity of the thermal response over the area that corresponded to the video acquisition window, we employed the red temperature probe M. The microplate heater was driven with 18 mA AC current at various frequencies from 0.02 to 2 Hz and the fluorescence signal was recorded over time with a charge-coupled device (CCD) camera. Then, by applying data treatment procedures similar to the ones used for detection in quadrature (vide infra), we obtained images where the gray levels were directly related to the average temperature as well as to the thermal excitation amplitude and phase (see Supporting Information). From the measurements displayed in Figure 4S in the Supporting Information, the three latter quantities could be assumed even over both the considered observation area and the investigated frequency range.

Fluorescence Microscopy and Video Acquisition. Imaging was achieved on the previously reported homemade dual-view epifluorescence microscope,[42] whose optics were arranged as follows. The source light was first passed through a multiband filter for selective excitation of both rhodamine green and Texas red (FF01-479/585−25; Semrock, Rochester, NY). A multiedge dichroic mirror (FF505/606-Di01; Semrock) and a 10× objective (Fluar NA 0.5; Zeiss, Le Pecq, France) were then used to perform epifluorescence illumination. The emitted light was subsequently collected and divided in two by a first 585DCXR dichroic mirror (Chroma Technology, Rockingham, VT). The resulting optical rays associated with the green (g) and red (r) channels were next filtered by relying respectively on FF01-525/30−25 and FF01-628/32−25 band-pass filters (Semrock). Finally, with the help of a second 585DCXR dichroic mirror, the two-color image was reconstructed on the chip of a CCD camera, either a BM-141 GE (JAI, Copenhagen, Denmark) or a Luca-R (Andor Technology, Belfast, U.K.). The field of view was ∼0.5 mm for each color channel. We could also estimate that, at similar dye concentrations, rhodamine green contamination accounted for less than 10% of the Texas red signal in the red acquisition window.

To derive an expression for the intensity of the images collected with the camera in each color channel c of the dual-view system, we consider a two-state exchange like that in eq 1. Fluorescence being emitted by both A_i species, after subtraction of the background signal, it yields

$$F^c(x,y,T) = E(x,y)\, C^c(x,y) \left[Q^c_{A_1} A_1(T) + Q^c_{A_2} A_2(T) \right] \quad (10)$$

where $E(x,y)$ is the illumination intensity arriving on the sample and $C^c(x,y)$ is the instrumental transfer function accounting for the collection of photons and their conversion in electrical signal.[42] Noticeably, E and C^c vary with the pixel coordinates, whereas concentration profiles in both reagent and product are here assumed to be homogeneous. In eq 10 the Q^c_{Ai} brightnesses are introduced, defined as

$$Q^c_{A_i} = \left[\int_\lambda 2.3\, e(\lambda)\, \varepsilon_{A_i}(\lambda)\, d\lambda \right] \times \left[\int_\lambda \phi_{A_i}(\lambda)\, c^c(\lambda)\, d\lambda \right] \quad (11)$$

where ε_{Ai} and ϕ_{Ai} are the A_i molar absorption coefficient and fluorescence quantum yield, respectively. On the other hand, the two functions e and c^c, whose integrals are equal to 1, hold for the variation with λ of the excitation and detection efficiencies, respectively. Finally, the 2.3 factor corresponds to ln 10; it originates from developing at first order the Beer−Lambert law to retrieve the intensity of light absorbed by the sample.[43] As demonstrated in a previous paper, E, C^c, and $Q_A{}^c$, as well as the total concentration $A = A_1 + A_2$, depend only weakly on T.[42]

In the case where a temperature modulation of small amplitude, $\beta T_0 \sin(\omega t)$, is applied around T_0, eq 10 can further be developed by use of eqs 3, 5, and 6. It is here important to remark that, as proved by the measurements reported in Figure 4S in the Supporting Information, both T_0 and β are even over the heater surface under study. Similarly, the thermal excitation shows no phase shift whatever the values of x and y. Thus, for experimental conditions that minimize photobleaching,[44] the temporal variation of the signal from each pixel is

$$F^c(x,y,t) = F^{c,0}(x,y) + \beta F^{c,1}(x,y) \sin(\omega t + \varphi^c + \phi) \quad (12)$$

dx.doi.org/10.1021/ac1026034 |Anal. Chem. 2011, 83, 2476–2484

with the angle ϕ reflecting the fact that the present setup does not allow us to precisely phase CCD recording and Joule heating. After $Z_A^{c,0}$ and $Z_A^{c,1}$ are introduced as[45]

$$Z_A^{c,0} = Q_{A_1}^c \frac{1}{(1+K_A^0)} + Q_{A_2}^c \frac{K_A^0}{(1+K_A^0)} \quad (13)$$

$$Z_A^{c,1} = \left(Q_{A_2}^c - Q_{A_1}^c\right) \frac{\Delta_A H}{RT_0} \frac{K_A^0}{(1+K_A^0)^2} \frac{1}{\sqrt{1+(\tau_A^0\omega)^2}} \quad (14)$$

the other terms of eq 12 are given by

$$F^{c,0}(x,y) = E(x,y)\, C^c(x,y)\, Z_A^{c,0} A \quad (15)$$

$$F^{c,1}(x,y) = E(x,y)\, C^c(x,y)\, Z_A^{c,1} A \quad (16)$$

$$\varphi^c = -\arctan(\tau_A^0\omega) \quad (17)$$

In general, video acquisition speed is restricted by the frequency of the camera: f_{video} = 30.1 and 36 Hz for the present BM-141 GE and Luca-R models, respectively. However, we chose to transfer at a constant rate only $2n$ frames per temperature oscillation, thus limiting the amount of data to be subsequently processed. For $\omega/2\pi \leq 0.375$ Hz, we typically set n at 8, yet its value had to be lowered in the case of faster modulations (for instance, down to 4 at $\omega_t^{res}/2\pi$ = 3.76 Hz). Furthermore, to improve the signal-to-noise ratio, recording was carried on over several periods; the number of collected images was ~250 for relaxation time measurements and ~5000 for quadrature detection. All the frames having the same index modulo $2n$ were next averaged together to yield a single oscillation-long movie. Therefore, thanks to eq 12, the intensity profile corresponding to the kth image is now given by

$$F^c(x,y,k) = F^{c,0}(x,y) + \beta F^{c,1}(x,y) \sin\left(\frac{k\pi}{n} + \varphi^c + \phi\right) \quad (18)$$

Incidentally, because an even number of images was regularly sampled over a period, one also has $\langle F^c(x,y,k)\rangle_k = F^{c,0}(x,y)$.

Using such a data collection protocol implied two experimental constraints. First, the camera and the temperature excitation frequencies had to be commensurable. More precisely, with an image pickup rate of $1/p$, two successive acquisitions were separated by a time lapse of p/f_{video} seconds. Thus, as $2n$ video frames were transferred per period of $2\pi/\omega$ seconds, it resulted in $\omega = \pi f_{video}/np$. The values accessible for the heating pulsation were in limited number and the function generator that drove the current flowing through the ITO resistor then had to be tuned accordingly. The second constraint was for the acquisition system to be able to collect and process a large number of video frames. We here relied on a homemade electronic setup, associated with a dedicated program written in C, to sort and average in real time the images sent by the CCD camera.

Relaxation Time Measurement. The $A_{t1} + P \rightleftharpoons A_{t2}$ dynamics was investigated by studying how a mixture of the corresponding molecules responds to small temperature oscillations. As we worked with an excess of probe,[46] the fluorescence signal collected in the green channel of the microscope, $F^g(x,y,k)$, thus obeyed the expressions derived for a two-state isomerization, that is, eqs12−18. In this experiment, artifacts related to thermal transfer caused us to also introduce in solution the molecular thermometer M (vide infra). It hence provided in the red video channel a response, $F^r(x,y,k)$, that similarly follows eqs 12−18.

Renormalizing the one-period-long movies by $\langle F^c(x,y,k)\rangle_k$ first enabled us to correct them from defects associated with inhomogeneous illumination and photon collection. After spatial averaging over a 125 × 150 pixels area, it resulted in two

$$F_{norm}^c(k) = 1 + \beta \frac{Z_A^{c,1}}{Z_A^{c,0}} \sin\left(\frac{k\pi}{n} + \varphi^c + \phi\right) \quad (19)$$

curves that could subsequently be fitted to sinusoids in order to provide the $\beta Z_A^{c,1}/Z_A^{c,0}$ amplitudes (Figure 2S, Supporting Information). Next, to get rid of the experimental bias linked to the variation of β with ω, we computed $\rho^{g/r}$ as the ratio between the green and red modulation depths: $\rho^{g/r} = (\beta Z_t^{g,1}/Z_t^{g,0})/(\beta Z_M^{r,1}/Z_M^{r,0})$. Indeed, this operation allowed us to obtain a function whose dependence on the angular frequency is contained only in a $1/[1 + (\tau_t^0\omega)^2]^{1/2}$ term (see Supporting Information). Finally, the relaxation time τ_t^0 was easily extracted by fitting the $\rho^{g/r}(\omega)$ transfer function (Figure 4b).

Quadrature Imaging. For the titration, the red-emitting molecular thermometer M was still added to the green-emitting sample to be analyzed. It therefore permitted access to the phase ϕ in a distinct color channel.

Adding the fluorescence issued from the various A_{li} species yields an oscillating signal, $F^g(x,y,k)$, whose amplitude in quadrature, $\beta F^{g,1cos}(x,y)$, is proportional to the sum of all the individual out-of-phase contributions, $(Q_{l2}^g - Q_{l1}^g)A_{l1}^{1cos}(x,y)$. To emphasize A_{t1}^{1cos}, we demodulated a one-period-long movie with a $-\pi/2$ phase delay.[24,25] More specifically, we first subtracted $\langle F^g(x,y,k)\rangle_k$ to the entire video. Then, we divided the resulting frames by a flat-field one, $F^{g,ff}(x,y)$, in order to correct them from optical artifacts (see Supporting Information for details). Finally, each image was multiplied by $\sin[(k\pi/n) + \phi - (\pi/2)]$ and the whole movie was averaged to give

$$F_{quad}^g(x,y) \propto \sum_l (Q_{l2}^g - Q_{l1}^g)\, A_{l1}^{1cos}(x,y) \quad (20)$$

Under the assumptions of similar concentrations, standard enthalpies of reaction, and brightness differences for all the reactive couples, the previous equation could further be transformed in $F_{quad}^g(x,y) \propto A_{t1}^{1cos}(x,y)$. Indeed, resonance conditions had been selected to selectively stress on $\{A_{t1}, A_{t2}\}$ and the interfering species were here such that $A_{l1}^{1cos}(x,y)$ was vanishing for $l \neq t$. Each pixel of the image therefore exhibited an intensity directly proportional to the A_t concentration and an absolute estimate for the latter could be obtained by relying on the channel 4 calibration standard (Figure 5).

Thermodynamic Parameters Measurement. The standard enthalpy and entropy of hybridization between the target and its probe, $\Delta_t H^P$ and $\Delta_t S^P$, were determined via a thermal denaturation experiment in which the temperature of the microscope stage was ramped from 10 to 45 °C and the green fluorescence emission from an $A_{t1} + P$ mixture was accordingly recorded. The two species being at respective initial concentrations A_t and yA_t, one can solve the mass action equation to obtain

$$\frac{F^g(T)}{F^g(318\,K)} = 1 + \left(\frac{Q_{t2}^g}{Q_{t1}^g} - 1\right) \times \frac{\left[(y+1)K_t^P A_t + 1\right] - \sqrt{\left[(y+1)K_t^P A_t + 1\right]^2 - 4y\left(K_t^P A_t\right)^2}}{2K_t^P A_t} \quad (21)$$

dx.doi.org/10.1021/ac1026034 |Anal. Chem. 2011, 83, 2476–2484

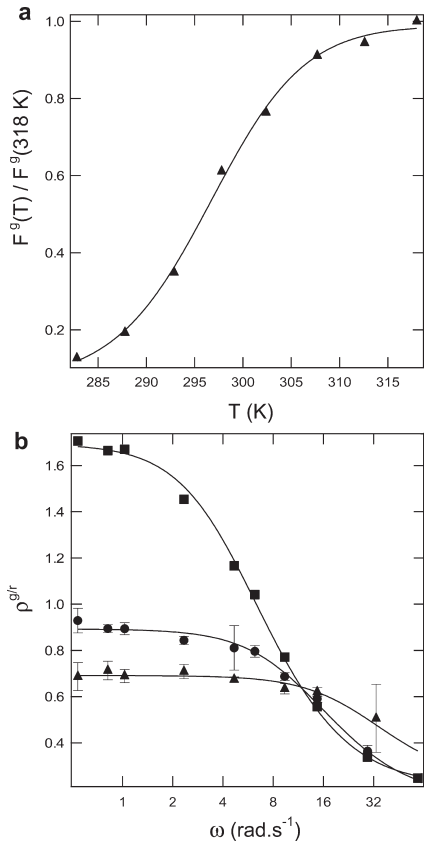

Figure 4. Thermokinetic characterization of the hybridization reaction between the A_{t1} target and the P probe. The fluorescence signal was collected in the green channel of the dual-view setup (λ_{exc} = 479 ± 19 nm, λ_{em} = 525 ± 15 nm) and measurements were performed on a solution obtained by mixing A_{t1} at 1 μM and P at 3 μM in 1.25 mM $Mg(OH)_2$, 25 mM NaOH, and 55 mM Hepes buffer, pH 7.5 at 20 °C, supplemented with 0.1% PDMA. (a) Temperature dependence of the fluorescence emission after normalization by its value at 318 K. (▲) Experimental data; (—) fit to eqs 21 and 22. (b) Dependence on the angular frequency of $\rho^{g/r}$, the ratio between the amplitudes of the green and red fluorescence signal modulations. M was here added in solution at 2 μM for normalization purposes and its emission was acquired in the red channel of the microscope (λ_{exc} = 585 ± 14 nm, λ_{em} = 628 ± 16 nm). Symbols correspond to the experimental points collected at various T_0: (■) 296 K, (●) 301 K, and (▲) 306 K. Solid lines are fits to $\propto 1/[1 + (\tau_t^0\omega)^2]^{1/2}$.

The signal was here normalized by its value at 318 K where no A_2 is present (see Supporting Information). In the latter equation K_t^P is the $A_{t1} + P \rightleftharpoons A_{t2}$ equilibrium constant:

$$K_t^P = \exp\left(-\frac{\Delta_t H^P - T\Delta_t S^P}{RT}\right) \qquad (22)$$

Consequently, fitting the experimental data yielded the two sought for thermodynamic parameters (Figure 4a).

■ RESULTS AND DISCUSSION

To experimentally evaluate the "temperature modulation and quadrature detection" approach for detection in a mixture, we chose to selectively titrate a fluorescent oligonucleotide using a hybridization reaction, this analysis being performed in the presence of other compounds similarly labeled. More precisely, we targeted a rhodamine green-conjugated sequence, A_{t1}, which forms a much less fluorescent duplex, A_{t2}, with the unlabeled probe, P. As putative interfering species, we adopted two green-emitting oligonucleotides: A_{NR}, a labeled poly(thymidine) strand that can be considered as a representative nonreactive sequence, and A_{MB}, a molecular beacon presently envisaged as a reagent engaged in an exchange faster than the targeted one, although it yields a paired structure with a similar stability. Indeed, in the considered temperature range the opening−closing relaxation time of the latter species, τ_{MB}^0, has been measured below 1 ms[42] and its equilibrium constant, K_{MB}^0, lies between 0.5 and 5.[47] As we will see in the following, when P varies between 3 and 7 μM, the corresponding values for the probe−target couple are $\tau_t^0 \sim 30-300$ ms and $K_t^0 \sim 0.3-6$ (see Table 2S in the Supporting Information).

The samples to be analyzed were injected in the PDMS channels, 35 μm wide and 10 μm high, of a dedicated device (Figure 3).[35] Although thermal excitation can be obtained by IR laser heating,[26,34] we here relied on the Joule effect[36,37] since adequate resistor design easily allows one to both vary and monitor the temperature at the second time scale.[35,48] Moreover, as heat is dissipated in a transparent ITO film (a 340 μm large square feature microfabricated on the bottom glass substrate), our chip is fully compatible with epifluorescence imaging. Using a dual-view optical setup,[49] we could selectively titrate green-labeled species while mapping the temperature field with M, a red-emitting molecular thermometer that was designed after the previously published MB[42] and that responds instantaneously to any of the thermal excitations applied in the present work. The average temperature as well as the oscillations' amplitude and phase were proved uniform over the 100 μm × 300 μm observation area (Figure 4S, Supporting Information), demonstrating that thermal transfer can be satisfactorily engineered when this kind of resistive element is utilized in combination with a holder acting as a heat reservoir.

We first performed a series of preliminary measurements devoted to identify the resonance conditions associated with the $A_{t1} + P \rightleftharpoons A_{t2}$ titration. In fact, in the context of a bimolecular reaction and according to the criteria given in eq 7, we had to look for an angular frequency and a probe concentration that respectively verify $\omega_t^{res} = 1/\tau_t^0$ and $P_t^{res} = 1/K_t^{P,0}$, where $K_t^{P,0}$ is the pairing equilibrium constant at T_0. By employment of the microscope and its thermostated stage, the standard enthalpy $\Delta_t H^P$ and entropy $\Delta_t S^P$ of hybridization were extracted from the temperature dependence of the fluorescence issued from a solution containing the investigated complementary strands (Figure 4a). In 1.25 mM $Mg(OH)_2$, 25 mM NaOH, and 55 mM Hepes buffer, pH 7.5 at 20 °C and 0.1% PDMA, we derived $\Delta_t H^P = -170 \pm 20$ kJ·mol^{-1} and $\Delta_t S^P = -460 \pm 60$ J·K^{-1}·mol^{-1} between 283 and 318 K. Since $K_t^P = \exp[-(\Delta_t H^P - T\Delta_t S^P)/RT]$, these two thermodynamic parameters provide hybridization constants in the 10^5-10^6 range. Incidentally, from the same experiment we also retrieved the relative brightness of the duplex with respect to the oligonucleotide: $Q_{t2}^g/Q_{t1}^g = 0.12 \pm 0.02$. In a second step, we determined the corresponding association and dissociation rate constants by studying the response to a modulated temperature excitation of a $A_{t1} + P$ solution.[22,23,26,34] We relied on the microheater to generate a harmonic forcing of weak amplitude (β = 0.002−0.008) with ω between 0.54 and 59 rad·s^{-1}. After fluorescence signal oscillations at various pulsations were recorded (Figure 2S, Supporting Information), the relaxation time τ_t^0 was extracted from fitting the amplitude of the chemical

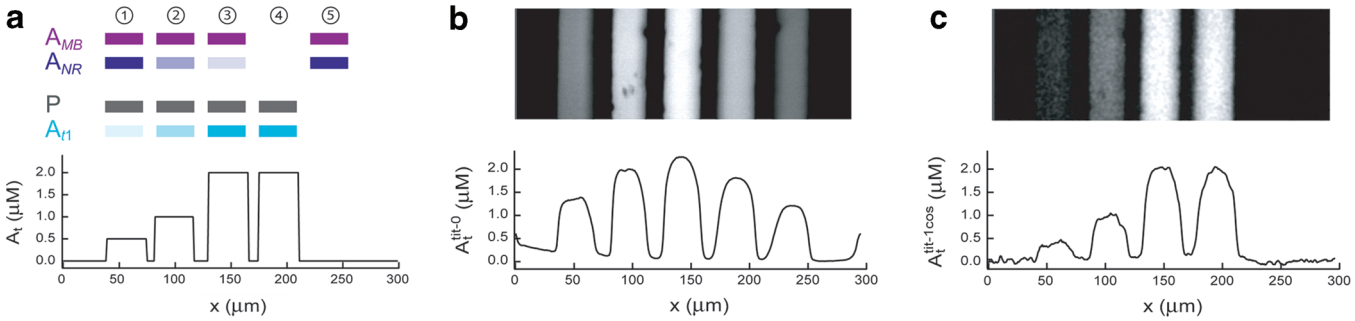

Figure 5. Titration of the A_{t1} target by the P probe in a mixture containing two interfering compounds, the nonreactive A_{NR} and the fast-exchanging A_{MB}. (a) Schematic representation of the various samples' initial composition and corresponding A_t profile; the complete set of concentration values is available in Table 3S in the Supporting Information. (b) Fluorescence emission at equilibrium at T_0 = 306 K and corresponding $A_t^{tit\text{-}0}$ trace. (c) Amplitude of the out-of-phase response upon harmonic forcing around T_0 and corresponding $A_t^{tit\text{-}1cos}$ trace. The temperature oscillations amplitude at ω_t^{res} = 23.65 rad·s^{-1} was βT_0 = 0.6 K and the probe concentration was P_t^{res} = 7 μM. Samples were prepared in 1.25 mM $Mg(OH)_2$, 25 mM NaOH, and 55 mM Hepes buffer, pH 7.5 at 20 °C, supplemented with 0.2% PDMA. Traces were computed by signal averaging along the image vertical axis and normalization by the channel 4 result.

system transfer function plotted in the frequency domain (Figure 4b). As $K_t^{P,0}$ could be derived from the results of the previous denaturation experiment, $k_{+t}^{P,0}$ and k_{-t}^{0} were next simply computed thanks to $K_t^{P,0} = k_{+t}^{P,0}/k_{-t}^{0}$ and $\tau_t^0 = 1/(k_{+t}^{P,0}P + k_{-t}^{0})$. The whole process was iterated at different average temperatures T_0, and the data were subsequently analyzed according to the Arrhenius law (Table 2S and Figure 3S, Supporting Information). In the 295−305 K range, τ_t^0 varies between 0.04 and 0.2 s and we found the following values for the activation energies and for the logarithms of the pre-exponential factors: E_{+t} = 48 ± 11 kJ·mol^{-1}, E_{-t} = 218 ± 11 kJ·mol^{-1}, ln r_{+t}^{P} = 33.4 ± 4.4, and ln r_{-t} = 88.7 ± 4.4. Now equipped with eq 7 and all the necessary kinetic parameters, we could look for conditions enabling the selective detection of A_{t1}. For various T_0, we estimated the resonant complementary strand concentration and excitation pulsation using $P_t^{res} = k_{-t}^{0}/k_{+t}^{P,0}$ and $\omega_t^{res} = k_{+t}^{P,0}P_t^{res} + k_{-t}^{0}$, respectively. Thereafter, we selected an average temperature that results in a large enough excess of probe with respect to the species to be titrated and in an angular frequency accessible to our experimental setup. At T_0 = 306 K, we could satisfactorily work with P_t^{res} = 7 μM and ω_t^{res} = 23.65 rad·s^{-1}.[50]

Figure 5a presents the different mixtures we injected in the microfluidic chip. Channels 1−3 contained increasing concentrations of the A_{t1} target, from 0.5 to 2 μM, at constant resonant concentration in the P complementary strand, 7 μM here. We also added in these solutions the two interfering compounds, the A_{NR} nonreactive sequence and the A_{MB} fast-exchanging beacon (their concentrations were in the micromolar range). In channel 4, we introduced the sole A_{t1} at 2 μM and P at 7 μM. In particular, this mixture was prepared to subsequently serve as a calibration standard, allowing the conversion into concentrations of the channels 1−3 responses. Yet we filled channel 5 with A_{NR} and A_{MB} only, in order to control the selectivity of our protocol. Importantly, we supplemented sample 4 with 2 μM of the red-emitting molecular beacon M to monitor the amplitude and phase of the temperature modulation.

The titration experiment was performed at T_0 = 306 K and with a β = 0.002 thermal forcing at angular frequency 23.65 rad·s^{-1}. Using a camera synchronized to the current generator, we recorded the fluorescence intensity variations in both green and red colors during 625 oscillations (166 s). Then, we converted the collected movie in a one-period-long video. First, complete time-averaging of the latter yielded the green image displayed in Figure 5b. It corresponds to the result that would be obtained without any thermal modulation, that is, when an equilibrium titration is performed at constant temperature T_0 (see Experimental Section). As expected from the close amounts of fluorescent label in solution, the emissions from the five channels were nearly similar. Furthermore, the extracted $A_t^{tit\text{-}0}$ values were clearly larger than the various target concentrations A_t. Subsequently, taking advantage of the knowledge of the temperature phase measured on the red image and relying on a phase-sensitive detection scheme,[23−25,51,52] we extracted for each pixel the amplitude of the green fluorescence oscillations in quadrature with the thermal excitation (see Experimental Section).[53] As shown in Figure 5c, the out-of-phase responses arising from the five channels were now different. The signal from sample 5, which did not include the sought for reactant, was completely extinguished. This observation agreed with the identical responses from channels 3 and 4, which contained the same amount of A_{t1} + P but with and without interfering compounds. In addition, the signal increased from samples 1 to 3, in line with the A_{t1} concentration variation. Thanks to the channel 4 standard, these data could even be quantitatively analyzed: we titrated 0.38 ± 0.1, 0.95 ± 0.1, and 2.03 ± 0.1 μM in target whereas 0.5, 1, and 2 μM had been introduced in solution.[54] Thus, the "temperature modulation and quadrature detection" protocol completely eliminated the contribution of the nonresonant species: in marked contrast with the results obtained upon titration at chemical equilibrium, it led to $A_t^{tit\text{-}1cos} \simeq A_t$.

CONCLUSIONS

Acquiring with a $\pi/2$ phase delay the signal originating from a mixture of two-state exchanging reactants submitted to a periodic thermal excitation allows one to discriminate—without any separation or washing step—a species of interest among various interfering compounds. Application to titration of what can be considered as a "thermokinetic band-pass filter" holds promises for selective and quantitative analyses. This approach has here been demonstrated by use of fluorescent microscopy, but it is generic. Whatever the observable (e.g., UV−vis or IR absorbance, refractive index), both limit-of-detection and dynamic range are at least the ones of the considered spectroscopy. Moreover, the present strategy will certainly be valuable when one has to look for minor components, a situation often

encountered in biology.[1,5,11] Resonant conditions are robust and easy to achieve as far as in vitro assays are concerned. In particular, an implementation to sensors and microarrays could particularly benefit the development of label-free detection techniques, the latter being presently hampered by experimental drifts and by a lack of selectivity with respect to nonspecifically adsorbed species.[12,14,27] Finally, compatibility with optical microscopy might be profitable in cell imaging, where contrast maps based on some specific biomolecule concentration should help to investigate reaction networks in vivo.

■ ASSOCIATED CONTENT

Supporting Information. Four figures, three tables, and additional text and equations describing the response of a two-state exchanging reactant submitted to a temperature modulation; measurement of thermodynamic parameters $\Delta_t H^P$ and $\Delta_t S^P$; the measurement of the relaxation time τ_t^0 and associated kinetic parameters; quadrature imaging; and temperature mapping with the molecular thermometer M. This material is available free of charge via the Internet at http://pubs.acs.org/.

■ AUTHOR INFORMATION

Corresponding Author

*E-mail: Thomas.Lesaux@ens.fr (T.L.S.); anle@lptmc.jussieu.fr (A.L.); charlie.gosse@lpn.cnrs.fr (C.G.); Ludovic.Jullien@ens.fr (L.J.).

■ ACKNOWLEDGMENT

This work was supported by two research fellowships from the Ministère de la Recherche et de la Technologie (to H.B. and E.C.) as well as grants "T-Wave" from the ANR blanche 2006 program and "T-ModSync" from the Cnano IdF 2008 program. We thank the LPN clean room and workshop staff for technical assistance.

■ REFERENCES

(1) Anderson, N. L.; Norman, N. G. *Mol. Cell. Proteomics* **2002**, *1*, 845–867.
(2) Gingeras, T. R.; Higuchi, R.; Kricka, L. J.; Lo, Y. M. D.; Wittwer, C. T. *Clin. Chem.* **2005**, *51*, 661–671.
(3) *Modern Methods of Drug Discovery*; Hillisch, A., Hilgenfeld, R., Eds.; Birkhaüser Verlag: Basel, Switzerland, 2003.
(4) Velculescu, V. E.; Zhang, L.; Zhou, W.; Vogelstein, J.; Basrai, M. A.; Basset, D. E., Jr.; Hieter, P.; Vogelstein, B.; Kinzler, K. W. *Cell* **1997**, *88*, 243–251.
(5) Holland, M. J. *J. Biol. Chem.* **2002**, *277*, 14363–14366.
(6) *Proteome Research*, 2nd ed.; Wilkins, M. R., Appel, R. D., Williams, K. L., Hochstrasser, D. F., Eds.; Springer-Verlag: Berlin, 2007.
(7) Noda, I.; Ozaki, Y. *Two-Dimensional Spectroscopy: Applications in Vibrational and Optical Spectroscopy*; Wiley: Chichester, U.K., 2004.
(8) Muller, M.; Buchet, R.; Fringeli, U. P. *J. Phys. Chem.* **1996**, *100*, 10810–10825.
(9) de Jong, L. A. A.; Uges, D. R. A.; Franke, J. P.; Bischoff, R. *J. Chromatogr. B* **2005**, *829*, 1–25.
(10) Sassolas, A.; Beca-Bouvier, B. D.; Blum, L. J. *Chem. Rev.* **2008**, *108*, 109–139.
(11) Draghici, S.; Khatri, P.; Eklund, A. C.; Szallasi, Z. *Trends Genet.* **2006**, *22*, 101–109.
(12) Ramachandran, N.; Larson, D. N.; Strak, P. R. H.; Hainsworth, E.; LaBaer, J. *FEBS J.* **2005**, *272*, 5412–5425.
(13) Ma, H.; Horiuchi, K. Y. *Drug Discovery Today* **2006**, *11*, 661–668.
(14) Bally, M.; Halter, M.; Vörös, J.; Grandin, H. M. *Surf. Interface Anal.* **2006**, *38*, 1442–1458.
(15) Eads, B.; Cash, A.; Bogart, K.; Costello, J.; Andrews, J. *Methods Enzymol.* **2006**, *411*, 34–49.
(16) Winkler-Oswatitsch, R.; Eigen, M. *Angew. Chem., Int. Ed.* **1979**, *18*, 20–49.
(17) Jullien, L.; Lemarchand, A.; Lemarchand, H. *J. Chem. Phys.* **2000**, *112*, 8293–8301.
(18) Alcor, D.; Croquette, V.; Jullien, L.; Lemarchand, A. *Proc. Natl. Acad. Sci. U.S.A.* **2004**, *101*, 8276–8280.
(19) Alcor, D.; Allemand, J.-F.; Cogné-Laage, E.; Croquette, V.; Ferrage, F.; Jullien, L.; Kononov, A.; Lemarchand, A. *J. Phys. Chem. B* **2005**, *109*, 1318–1328.
(20) Lemarchand, A.; Jullien, L. *J. Phys. Chem. A* **2005**, *109*, 5770–5776.
(21) Berthoumieux, H.; Jullien, L.; Lemarchand, A. *J. Phys. Chem. B* **2007**, *111*, 2045–2051.
(22) Eigen, M.; de Mayer, L. In *Relaxation Methods in Techniques of Organic Chemistry*, 2nd ed.; Friess, S. L., Lewis, E. S., Weissberger, A., Eds.; Wiley: New York, 1963; Vol. 8, Part 2, pp 895−1054.
(23) Fringeli, U. P.; Baurecht, D.; Günthard, H. H. In *Infrared and Raman Spectroscopy of Biological Materials*; Gremlich, H.-U., Yan, B., Eds.; Marcel Dekker: New York, 2000; pp 143−191.
(24) Baurecht, D.; Fringeli, U. P. *Rev. Sci. Instrum.* **2001**, *72*, 3782–3792.
(25) Urakawa, A.; Bürgi, T.; Baiker, A. *Chem. Eng. Sci.* **2008**, *63*, 4902–4909.
(26) Braun, D.; Libchaber, A. *Appl. Phys. Lett.* **2003**, *83*, 5554–5556.
(27) Williams, L. D.; Ghosh, T.; Mastrangelo, C. H. *Anal. Chem.* **2010**, *82*, 6025–6031.
(28) Berthoumieux, H.; Jullien, L.; Lemarchand, A. *Phys. Rev. E* **2007**, *76*, No. 056112.
(29) Berthoumieux, H.; Antoine, C.; Lemarchand, A. *J. Chem. Phys.* **2009**, *131*, No. 084106.
(30) Berthoumieux, H.; Antoine, C.; Jullien, L.; Lemarchand, A. *Phys. Rev. E* **2009**, *79*, No. 021906.
(31) SantaLucia, J.; Allawi, H. T.; Seneviratne, P. A. *Biochemistry* **1996**, *35*, 3555–3562.
(32) Strazewski, P. *J. Am. Chem. Soc.* **2001**, *124*, 3546–3554.
(33) Weber, P. C.; Salemme, F. R. *Curr. Opin. Struct. Biol.* **2003**, *13*, 115–121.
(34) Schoen, I.; Krammer, H.; Braun, D. *Proc. Natl. Acad. Sci. U.S.A.* **2009**, *106*, 21649–21654.
(35) Barilero, T.; Chapuis, P.-O.; Pujade, D.; Guilet, S.; Croquette, V.; Jullien, L.; Volz, S.; Gosse, C. Digest of the Technical Papers, Transducers '07 & Eurosensors XXI: 14th International Conference on Solid-State Sensors, Actuators and Microsystems, Lyon, France, June 10−14, 2007; pp U933−U934
(36) Verpoorte, E.; de Rooij, N. F. *Proc. IEEE* **2003**, *91*, 930–953.
(37) Gosse, C.; Bergaud, C.; Löw, P. In *Thermal Nanosystems and Nanomaterials*; Volz, S., Ed.; Springer-Verlag: Berlin, 2009; pp 301−341.
(38) Kato, H.; Nishizaka, T.; Iga, T.; Kinosita, K.; Ishiwata, S. *Proc. Natl. Acad. Sci. U.S.A.* **1999**, *96*, 9602–9606.
(39) Hamad-Schifferli, K.; Schwartz, J. J.; Santos, A. T.; Zhang, S.; Jacobson, J. M. *Nature* **2002**, *415*, 152–155.
(40) Stehr, J.; Hrelescu, C.; Sperling, R. A.; Raschke, G.; Wunderlich, M.; Nichtl, A.; Heindl, D.; Kürzinger, K.; Parak, W. J.; Klar, T. A.; Feldmann, J. *Nano Lett.* **2008**, *8*, 619–623.
(41) Actually, discrimination between two-state exchanging reactants is nearly impossible if the response exhibits no absolute extremum. Such a situation is encountered, for instance, when one considers the in-phase term $A_1^{1\sin}$, the equilibrium one A_1^0, as well as the amplitude $A_1^1 = [(A_1^{1\sin})^2 + (A_1^{1\cos})^2]^{1/2}$ and phase $\varphi = -\arctan(\tau^0\omega)$ of the concentration modulation (see Figure 1a and Figure 1S in the Supporting Information).
(42) Barilero, T.; Le Saux, T.; Gosse, C.; Jullien, L. *Anal. Chem.* **2009**, *81*, 7988–8000.
(43) Valeur, B. *Molecular Fluorescence: Principles and Applications*; Wiley−VCH: Weinheim, Germany, 2002.

(44) We did not notice any significant decrease in the amplitude of the fluorescent oscillations during the course of the measurements. The photochemical half-life associated with the present illumination settings and the present chromophores is thus several times larger than the duration of our longest acquisition, that is, ∼390 s.

(45) Contrary to what has been done for the sake of readability in the Theory section, we here clearly indicate with a subscript A that the thermokinetic parameters are the ones associated with the $A_1 \rightleftharpoons A_2$ reaction. More concise notations will be adopted when several $\{A_{l1}, A_{l2}\}$ reactive couples will be mixed together. For instance, $Z_l^{c,0}$ will be used instead of $Z_{A_l}^{c,0}$ and Q_{l1}^c instead of $Q_{A_l1}^c$.

(46) Although P is here introduced at a concentration just 3 times higher than A_{t1}, the "large excess" assumption holds because it yields no significant discrepancy with respect to the exact τ_t^0 computation. More precisely, the present simplification, that is, $\tau_t^0 = 1/(k_{+t}^{P,0}P + k_{-t}^0)$ with $P = 3\ \mu$M, introduces a systematic error that has been estimated to be less than ∼5%; conversely, uncertainties on experimental data can be up to 20% (see Table 2S in the Supporting Information for examples).

(47) This estimate is based on $\Delta_{MB}H = -136\ \text{kJ}\cdot\text{mol}^{-1}$ and $\Delta_{MB}S = -450\ \text{J}\cdot\text{K}^{-1}\cdot\text{mol}^{-1}$, values for the standard enthalpy and entropy of folding which are given in Barilero, T. *Imagerie de la Cinétique Chimique par Modulation de Température: Conception, Validation et Mise en œuvre*. Ph.D. thesis, Université Pierre et Marie Curie, Paris, 2009.

(48) Arata, H. F.; Rondelez, Y.; Noji, H.; Fujita, H. *Anal. Chem.* **2005**, *77*, 4810–4814.

(49) Kinosita, K.; Itoh, H.; Ishiwata, S.; Hirano, K.; Nishizaka, T.; Hayakawa, T. *J. Cell Biol.* **1991**, *115*, 67–73.

(50) These experimental conditions are not exactly equal to the resonance ones. Indeed, the kinetic data extracted from Figure 3S in the Supporting Information leads to $P_t^{res} = 1/K_t^{P,0} = 10.2\ \mu$M and $\omega_t^{res} = k_{+t}^{P,0}P_t^{res} + k_{-t}^0 = 37.72\ \text{rad}\cdot\text{s}^{-1}$ at 306 K. Thus, rigorously, we should have used the latter probe concentration and excitation pulsation. However, only a limited number of frequencies are accessible to our video acquisition setup (see Experimental Section) and we were obliged to retain slightly different settings. Nevertheless, selective titration could be achieved thanks to the nonzero bandwidth of the filter function displayed in Figure 1b.

(51) McGown, L.; Bright, F. *Anal. Chem.* **1984**, *56*, 1400A–1417A.

(52) Scofield, J. H. *Am. J. Phys.* **1994**, *62*, 129–133.

(53) Phase-sensitive detection (PSD) is recognized to be a narrow-band technique allowing the elimination of noise at frequencies that are distinct from the excitation one.[24−27] However, it is here implemented numerically using a limited sampling rate in the time domain; thus, we do not know to what extent we still benefit from the latter advantage. We are presently developing an analogical PSD relying on a modulated illumination, as described by Braun and Libchaber,[26] and we will therefore soon be able to compare the signal-to-noise ratios provided by both approaches.

(54) The precision of the titration can be estimated by computing the standard deviation of the pixel intensity over the microfluidic channel surface. Even if values around 0.01 μM were found, we have decided to display 10 times larger error bars. Indeed, we noticed that sometimes measurement accuracy was degraded by experimental issues such as the presence of dust or imperfect matching between the titration image and the flat-field one.